The Oxidizing Capacity of the Earth's Atmosphere: Probable Past and Future Changes

Anne M. Thompson

The principal oxidants in the lower atmosphere are ozone (O_3) and two by-products of O_3 photodissociation, the hydroxyl radical (OH) and hydrogen peroxide (H_2O_2). A number of critical atmospheric chemical problems depend on the earth's "oxidizing capacity," which is essentially the global burden of these oxidants. There is limited direct evidence for changes in the earth's oxidizing capacity since recent preindustrial times when, because of industrial and population growth, increasing amounts of O_3 precursor trace gases (carbon monoxide, nitrogen oxides, and hydrocarbons) have been released into the atmosphere. The concentrations of O_3 and possibly H_2O_2 have increased over large regions. Models predict that tropospheric O_3 will increase ~0.3 to 1% per year over the next 50 years with both positive and negative trends possible for OH and H_2O_2. Models and the observational network for oxidants are improving, but validation of global models is still at an early stage.

The earth's atmosphere is an oxidizing atmosphere. The principal oxidants are O_3, the OH radical, and H_2O_2. Each of these constituents reacts chemically with different species and plays an important role in the atmosphere. The concentration of O_3 is used to assess regional air quality (*1*). Concentrations of O_3 range from a few parts per billion by volume (ppbv) in less polluted areas to more than 100 ppbv in areas polluted by industrial activity or burning of biomass. Much of the current interest in global distributions of tropospheric O_3 stems from the effectiveness of mid- to upper tropospheric O_3 as a greenhouse gas (*2*).

The OH radical has been referred to as the "tropospheric vacuum cleaner" (*3*) because it reacts with hundreds of gases, both natural and anthropogenic. It controls the buildup of pollutants, including the hydrogenated chlorofluorocarbons now being adopted as substitutes for the pure chlorofluorocarbons. This suggests that it is desirable to maintain healthy atmospheric concentrations of this oxidant. On the other hand, higher concentrations of OH lead to more rapid formation of acids that deposit on the earth's surface directly or in precipitation. Nitrogen and sulfur oxides are converted, respectively, to nitric and sulfuric acid; nonmethane hydrocarbons (NMHC) are oxidized to organic acids after reaction with OH. Hydrogen peroxide also contributes to acid precipitation because it is the oxidant that converts SO_2 to sulfuric acid in cloud and rain droplets at low pH (*4*).

Thus, O_3, OH, and H_2O_2 are key players in a number of environmental problems, and there is considerable interest in whether their atmospheric concentrations are changing over time. The total atmospheric burden of O_3, OH, and H_2O_2 determines the "oxidizing capacity" of the atmosphere (*5*). As a result of the multiple interactions among the three oxidants and the multiphase activity of H_2O_2, there is no single expression that defines the earth's oxidizing capacity (*6*). Some researchers take the term loosely to mean the total global amount of OH, although even this parameter is not defined unambiguously (*7*).

In this article, I describe the atmospheric chemistry of O_3, OH, and H_2O_2 and present observational evidence for historical changes in each of the oxidants. Photochemical models are used to interpret the oxidant record in terms of changing atmospheric concentrations of other trace gases (for example, CH_4 or CO) or changing climatic properties. These models are also used to predict concentrations of O_3, OH, and H_2O_2 over the next 50 to 100 years.

The author is with the National Aeronautics and Space Administration (NASA) Goddard Space Flight Center, Laboratory for Atmospheres, Greenbelt, MD 20771.

Oxidants in Atmospheric Chemistry

Ozone, OH, and H_2O_2 interact with each other and with other key trace gases in a variety of ways (Fig. 1). Ozone interconverts atmospheric odd nitrogen (NO, NO_2, NO_3), hydrogen (OH and HO_2), halogens, and sulfur and readily oxidizes unsaturated hydrocarbons. The major photochemical loss process for O_3 in the troposphere (0 to 15 km) leads to formation of the OH radical. This occurs by way of reaction between the transient $O(^1D)$ and water vapor, following formation of $O(^1D)$ from O_3 by photodissociation in the near-ultraviolet:

$$O_3 + h\nu \rightarrow O(^1D) + O_2 \quad \text{(R1)}$$

$$O(^1D) + H_2O \rightarrow OH + OH \quad \text{(R2)}$$

Hydrogen peroxide forms when two HO_2 radicals combine, either in the atmosphere or inside droplets (*8*):

$$OH + O_3 \rightarrow HO_2 + O_2$$

$$HO_2 + HO_2 \rightarrow H_2O_2 + O_2 \quad \text{(R3)}$$

Although the formation of OH follows the destruction of O_3 (R1 and R2), subsequent reactions of OH can lead to O_3 formation by conversion of NO to NO_2 (*9*):

$$OH + CH_4\ (+O_2) \rightarrow CH_3O_2 + H_2O \quad \text{(R4)}$$

or

$$OH + CO\ (+O_2) \rightarrow CO_2 + HO_2 \quad \text{(R5)}$$

followed by

$$CH_3O_2 + NO \rightarrow NO_2 + CH_3O \quad \text{(R6)}$$

or

$$HO_2 + NO \rightarrow NO_2 + OH \quad \text{(R7)}$$

$$NO_2 + h\nu \rightarrow O + NO \quad \text{(R8)}$$

$$O + O_2\ (+M) \rightarrow O_3 + M \quad \text{(R9)}$$

With reactions R1 through R9 occurring simultaneously, the processes in R4 and R5 do not represent 100% losses for OH. In regions with sufficient concentrations of reactive NMHC from pollution or from vegetative emission of isoprene, an OH oxidation analogous to R4 produces an organic peroxy radical, RO_2 that can also convert NO to NO_2 (R7), leading to O_3 formation. In a low-NMHC environment

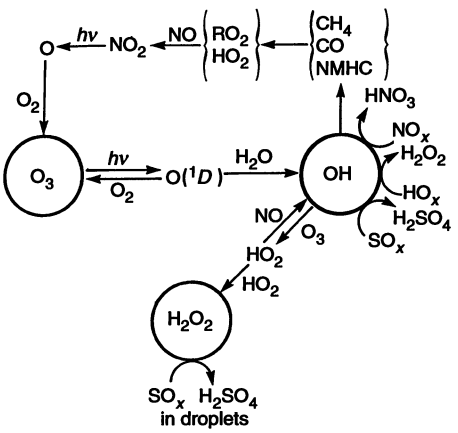

Fig. 1. The roles of the oxidants O_3, OH, and H_2O_2 in atmospheric photochemical reactions.

(usually polar or remote marine regions), up to 75% of OH loss is by reaction with CO and the remainder with CH_4.

In that atmospheric CH_4 is increasing globally, currently at a rate of 0.5 to 1% per year (*10, 11*), the chain of reactions R1 to R9 suggests that, even if the concentrations of other trace gases did not change, increasing emissions of CH_4 could be perturbing background concentrations of O_3, OH, and H_2O_2 (*12–16*). Ozone would be expected to increase in response to higher concentrations of CH_4.

The tendencies for OH and H_2O_2 to change as CH_4 (or CO, NO, or NMHC) emissions increase depend on unperturbed CO, hydrocarbon, and NO_x concentrations because of feedbacks among these species. Consider the reactions that determine the equilibrium concentration of OH:

$$OH \sim \frac{[O(^1D)][H_2O]}{k_{R4}[CH_4] + k_{R5}[CO] + \sum_i {}'k_i\,[NMHC_i]}$$

where the k's represent rate coefficients for reactions between OH and the species that it oxidizes (*17*). The denominator shows that NMHC and CO suppress OH concentrations in the initial oxidation, but subsequent reactions formed in those processes produce O_3, which contributes to OH via R1 and R2. In particular, NO concentrations are pivotal in CH_4-CO-hydrocarbon-O_3-OH feedbacks. If sufficient NO is present to make the processes in R6, R7 (and analogous reactions with oxygenated hydrocarbons) efficient, O_3 may be formed sufficiently fast for OH formation to dominate as CH_4 emissions increase.

Thus, the formation of oxidants is complex, with tropospheric OH and O_3 concentrations depending nonlinearly with simultaneously varying emissions (surface fluxes) of CH_4 and NO. This complicates calculation of oxidant concentrations by photochemical models, particularly those that simulate an urban-influenced environment. Consider a model in which NO_x ranges from 1 to 2 ppbv and unperturbed O_3 is 60 ppbv (Fig. 2A). With higher emissions of NO, an increasing CH_4 flux adds to tropospheric OH. However, beyond a certain point, increasing NO emissions suppress OH because removal of OH by NO_2 to form HNO_3 becomes effective:

$$OH + NO_2 + M \rightarrow HNO_3 + M \quad (R10)$$

Nitric acid, with a photochemical lifetime of several days, is a reservoir for OH and NO_2, which otherwise cycle in a matter of seconds between HO_2 and NO, respectively (Fig. 1). At very low surface NO fluxes (as in a remote marine tropical environment), additional CH_4 emissions suppress OH concentrations under nearly all conditions (Fig. 2B).

Beyond a certain concentration of NO_x, O_3 production also becomes less efficient (*18, 19*) and is further complicated by the presence of hydrocarbons. Atmospheric hydrocarbon concentrations range from low levels in the marine atmosphere (total NMHC as an equivalent amount of carbon is <1 ppbv C, consisting of low molecular weight alkanes and alkenes) to hundreds of parts per billion by volume C in an urban area (for example, alkanes, alkenes, and aromatics from combustion) or in a forested region (isoprene that is very reactive with OH and terpenes).

Modeling Atmospheric Oxidants

Evaluation of past and future oxidant trends requires photochemical models that can simulate changes in O_3, OH, and H_2O_2 concentrations under the influence of changing emissions of trace gases (CO, NO, NMHC, for example) on a global scale. The chemical reactions and physical processes in a model are considered valid for making future predictions if they reproduce present observations and past trends. For example, photochemical reaction schemes with hundreds of processes involving hydrocarbons and their oxidation by-products can be validated in regional-scale models that have been developed to devise pollutant control strategies (*20*). Experiments conducted in smog chambers provide some constraint, but so far there is no single "best" set of chemical reactions. Thus, each model uses the reaction scheme that best simulates the constituent of interest, for example, O_3 in air quality models and H_2O_2 for acid deposition models.

Models are further complicated when oxidant reactions in condensed phases (for example, aerosols, cloud, rain droplets) and on particle surfaces are introduced into the reaction scheme (*21*). Simulations show that cloud scavenging of free radicals may significantly modify oxidant concentrations (*22*), but there are not sufficient observations to confirm this. Mechanistic complexities imply inherent uncertainties in calculating concentrations of O_3, OH, and H_2O_2. Even the relatively uncomplicated models that are used to simulate nonpolluted environments (20 to 30 trace species and fewer than 100 photochemical reactions) propagate imprecisions from reaction rate coefficients as measured in the laboratory (*23, 24*). One study suggests that kinetic uncertainties in a typical CH_4-CO-OH-NO_x-O_3 reaction scheme introduce ~25% uncertainty into a calculation of the global OH concentration (Fig. 3).

Calculations of oxidant changes have been conducted with one- (1D), two- (2D), and three-dimensional (3D) models. The 1D models give only vertical profiles of trace gases and are useful for determining the sensitivity of chemical composition to changes in emissions or to other processes that are reasonably parameterized to one dimension (for example, radiation). Several 1D models compute regional changes in O_3, OH, and H_2O_2 for different types of chemical environments (*15, 25*) and average over the regions to estimate global oxidant changes.

The 2D models treat latitudinal variations in atmospheric variables (mixing times, temperature, moisture, solar insolation, stratospheric injection of O_3 and odd nitrogen, source strengths) with zonally averaged parameters (*26–30*). This approach is inadequate for representing extremes in emissions of short-lived nitrogen oxides and hydrocarbons and their subsequent O_3 formation (*31*). A recent study with a 3D model demonstrated that zonally averaging NO_x and hydrocarbon emissions may overestimate O_3 and OH concentrations in the low-altitude tropics and at northern midlatitudes (*32*). The OH overestimate implies an underestimate in the amount of CH_4, for

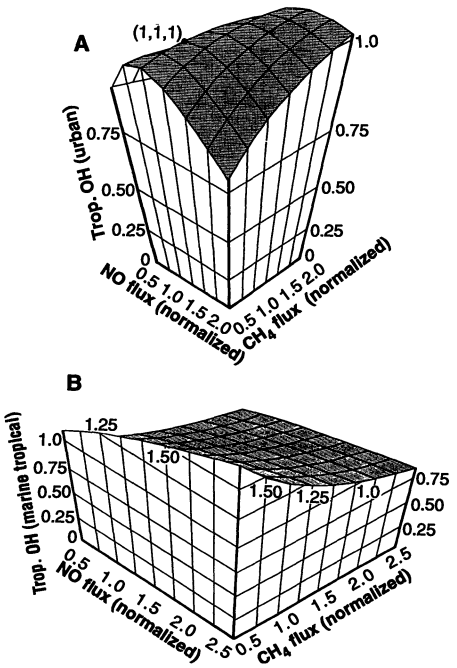

Fig. 2. Tropospheric OH response to changes in CH_4 and NO emissions. Tropospheric OH is defined as the total column abundance between the surface and 15 km. (**A**) Initial conditions (1,1,1) correspond to a composition typical of urban-influenced mid-latitude regions: ~60 ppbv O_3, 1.4 ppbv NO_x (NO_x = NO + NO_2); 380 ppbv CO. (**B**) Initial conditions (1,1,1) correspond to a composition typical of marine tropics: ~20 ppbv O_3, 5 pptv NO, 90 ppbv CO. Normalized CH_4 fluxes are 8×10^{10} cm^{-2} s^{-1} for the urban region and 1×10^{11} cm^{-2} s^{-1} for the marine region. Normalized NO fluxes at (1,1,1) are 7×10^{10} cm^{-2} s^{-1} for the urban region and 7×10^{8} cm^{-2} s^{-1} for the marine region. [Reprinted with permission from (*18*); Pergamon Press]

which OH is the dominant photochemical sink. This would lead to an error in a climate model that calculates radiative forcings from specified concentrations of CH_4 and other greenhouse gases (*33*).

The 3D models offer the potential of more accurate simulation of oxidants because they can resolve regions of extreme chemical source variability and other physical characteristics for which longitudinal averaging is probably not meaningful, for example, convection (*34*), cloudiness, precipitation, and surface uptake rates. Even so, for model integrations over long time periods (for example, to look at O_3 and OH and their interactions with climate) processes on scales smaller than the physical grid of the model must be parameterized.

Probable Past Oxidant Changes

Ozone. Although it is obvious that urban regions of high O_3 are a relatively recent and widespread phenomenon, from the viewpoint of global oxidizing capacity O_3 concentrations in nonurban (background) locations and in the free troposphere are of most interest. Observations rarely predate the 1960s, although records of surface O_3 made in the last century at nonurban Western Europe and North American sites show clear evidence for long-term changes in O_3 concentrations in these places. For example, the monthly mean concentration of surface O_3 recorded at Montsouris outside Paris in the 1870s to 1880s (*35, 36*) was half as high as nonurban O_3 means from background sites in the 1970s and 1980s in Canada, the United States, and Germany during winter and 1/3 to 1/5 as high during summer (Fig. 4).

The modern record from which global tropospheric O_3 trends are derived is taken from surface monitoring at a few sites and from vertical profiles collected at roughly two dozen locations at varying intervals by balloon- or rocket-borne ozonesondes (*37*). Surface O_3 has been monitored continuously at the four baseline sites of the National Oceanic and Atmospheric Administration (NOAA) Climate Monitoring and Diagnostics Laboratory (CMDL) since about 1960 (Fig. 5). The two Northern Hemisphere sites show increases in surface O_3 from 1974 to 1989 (*37*), but the increases at Mauna Loa may be only apparent. The trend [+(0.43 ± 0.34)% $year^{-1}$ from 1974 to 1989] nearly disappears when the maxima from 1981 to 1983 maxima are discounted. At Point Barrow the strongest positive trend occurs for measurements in July, as would be expected from the interaction of increasing levels of pollutants with maximum solar insolation, but O_3 concentrations have also increased in autumn during lower insolation.

At the South Pole CMDL site, surface O_3 has been decreasing at an increasing rate (Fig. 5). The trend for 1974 to 1989 is $-(0.38 \pm 0.27)\%$ $year^{-1}$, but summertime O_3 decreased by 15 to 20% from 1976 to 1989, apparently as a result of stratospheric O_3 depletion during austral spring and summer (*38*). Stratospheric O_3 depletion allows more than normal amounts of ultraviolet

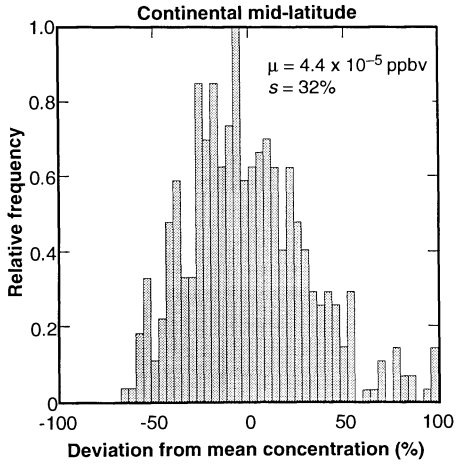

Fig. 3. The fractional uncertainty [$s = (1\sigma/\mu) \times 100$] in the computed OH concentration from a Monte Carlo study with a 1D photochemical model (*24*). The distribution of OH mixing ratios from 400 model runs is shown. Mixing ratios for 24 species (some illustrated in Fig. 1) are computed in every run. For each constituent the continuity equation includes nonvarying transport and photochemical production and loss terms from among 73 reactions (free radical formation, propagation, and recombination processes). In every simulation the rate coefficient for each process is chosen randomly from recommended values based on laboratory measurements. Mean values and 1σ imprecisions for the coefficients are given in (*23*). There are 24 processes in the model involving reaction with OH. The fractional uncertainty varies with the mean value, that is, atmospheric conditions. The case shown is based on mean O_3, NO_x, and CO conditions for a nonpolluted continental environment. In a more polluted environment the fractional uncertainty in OH may exceed 60%.

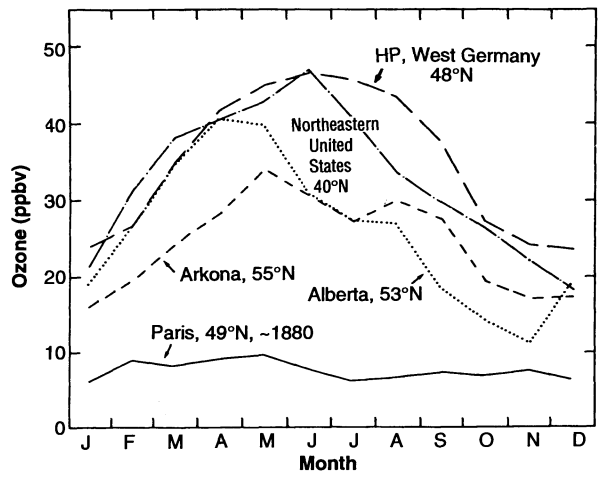

Fig. 4. A comparison of monthly mean surface O_3 mixing ratios from the 1970s and 1980s compared to observations from Montsouris, France, in the 1880s (*36*). The weak maximum in the Montsouris record is evident during spring when dynamical exchange of O_3 from stratosphere to troposphere is most active. In the modern-day record, the maximum (*79*) has shifted to July when the peak in solar ultraviolet insolation occurs, and the amount of O_3 produced in the lower atmosphere from reactions of combustion-derived CO, NO_x, and hydrocarbons exceeds the amount of O_3 transported downward from the stratosphere. [From (*80*) as reported in (*33*)]

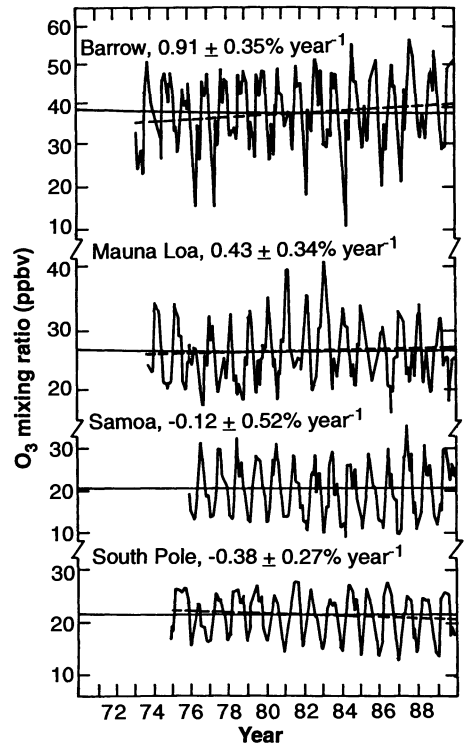

Fig. 5. Monthly mean surface O_3 at four CMDL stations (*81*) showing trends (dashed lines) from 1973 to 1989. Trends from 1973 to 1989 are superimposed on monthly mean O_3 mixing ratios. The variation in seasonal behavior among the four sites reflects local differences in photochemistry, stratosphere-troposphere exchange processes, and deposition to the surface. [After (*37*)]

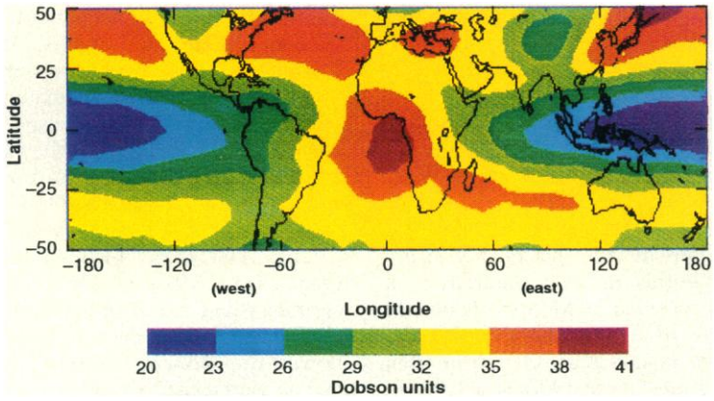

Fig. 6. Tropospheric residual O_3 (annual mean distribution) from TOMS and SAGE satellite observations (*43*). Note the maximum in the tropics west of Africa as well as high values in northern mid-latitude industrialized regions.

light to penetrate to the troposphere (*39*). This leads to tropospheric O_3 destruction (R1), which is not offset by O_3-forming processes (R4 through R9) because concentrations of NO_x are too low at the South Pole (*40*). Surface O_3 depletion at the South Pole may be the first evidence that stratospheric O_3 depletion is modifying tropospheric O_3 (*41*).

Ideally, global monitoring of a highly variable gas such as O_3 is done from space. Although tropospheric O_3 is not directly measured from any currently operational satellite, a method of using satellite data to deduce the total thickness of tropospheric O_3 has been developed by Fishman and co-workers (*42*). The technique is applicable between 50°N and 50°S where the TOMS (Total Ozone Mapping Spectrometer aboard Nimbus 7) gives "total" O_3 between the top of the atmosphere and the earth's surface and the SAGE instrument (Stratospheric Aerosols and Gases Experiment aboard the Earth Radiation Budget satellite) gives the stratospheric O_3 column. The difference between column O_3 from TOMS and stratospheric O_3 as registered by SAGE is called the "tropospheric residual," usually reported in Dobson units (DU; one DU = 2.69×10^{16} molecules of O_3 per square centimeter) (*43*). The tropospheric residual is a good approximation to the total depth of tropospheric O_3 and correlates well with ozonesonde measurements at the mid-tropospheric level, that is, 500 mbar (*42*).

The tropospheric residual (Fig. 6) gives a remarkable picture of global distributions and seasonal patterns of O_3. In particular, measurements from 1979 to 1990 show that the highest values of the tropospheric residual (35 DU or more) were confined to northern mid-latitudes (25° to 50°N), except for a region in the tropics west of Africa. Distinct seasonal changes are evident in both the Northern Hemisphere and the Southern Hemisphere. The maximum in the Northern Hemisphere occurs in July with values >40 DU found over Europe and downwind of Asia. The principal cause, as sonde and surface O_3 records suggest, is widespread industrial pollution. In the Southern Hemisphere tropospheric O_3 residuals are highest during the austral late winter and spring, possibly as a result of a large influx of O_3 from the stratosphere. From September to November, however, the highest tropospheric O_3 residual in the Southern Hemisphere is found off the African coast; it may be associated with urban pollution and the burning of biomass on the African and South American continents (*43*, *44*). The satellite data suggest that the tropical burning source of O_3 may be increasing (*44*). The apparent tropospheric O_3 increase may account for the lack of a negative total O_3 (stratosphere + troposphere) trend as derived from TOMS (*45*).

The OH radical. To many researchers the questions of changing oxidizing capacity and changes in global OH are synonymous because the total amount of OH determines the atmospheric lifetime of gases such as CH_4 and hydrogenated chlorofluorocarbons that are greenhouse gases and interact with stratospheric O_3 (*46*). Thus, models that predict tropospheric O_3 forcings on global climate and O_3 depletion depend critically on being able to determine OH changes. However, with a mean concentration of $\sim 10^6$ molecules cm^{-3} (approximately one in 50 trillion), OH is too dilute to measure except in isolated conditions by long-path length absorption (*47*) or complex laser techniques (*48*). Thus, direct monitoring of OH is not practical.

Two approaches to tracking trends in global OH are used: (i) models that compute OH from a fairly complete set of chemical reactions, assuming changing concentrations or emissions of more stable gases; (ii) a network of observations called the Atmospheric Lifetime Experiment (ALE) and its successor, the Global Atmospheric Gases Experiment (GAGE), that define an experiment from which OH can be derived with a suitable model (*49*). The idea of the ALE and GAGE experiments is simple. Select a manufactured trace gas with well-defined sources that reacts with OH at a known rate and monitor concentrations of the compound over time at a series of background stations. The compound is 1,1,1-trichloroethane (CH_3CCl_3, commonly called methyl chloroform), and five background stations have been used since the late 1970s. Using the first 7 years of ALE-GAGE data, Prinn and co-workers (*49*) derived a global OH concentration of

Table 1. Model-calculated changes in global OH. AREAL, Atmospheric Research and Exposure Assessment Laboratory; OGI, Oregon Graduate Institute; GSFC, Goddard Space Flight Center; n.a., not available; NH, Northern Hemisphere; SH, Southern Hemisphere.

Model and type	Reference	Current global OH (10^6 cm^{-3})*	OH change since preindustrial time	OH change since LGM
Harvard University (1D)	(*56*)	n.a.	60% loss	150% loss†
Cambridge University (2D)	(*30*)	0.95	NH: 50% loss SH: 20% gain	
Max Planck (2D)	(*82*)	0.91	NH: 50% gain to 40% loss SH: 20–40% loss	30–40% loss
Max Planck (3D)	(*83*)	0.6–0.80	NH: 10–20% gain SH: 10–20% loss	
USEPA/AREAL (1D)	(*55*)	0.6	4% loss	20% loss
OGI (multi-1D)	(*25*)	0.8	11% loss	40% loss
GSFC (multi-1D)	(*53*)	0.6	20% loss	32% loss

*Global average refers to volume average over model domain. †LGM calculation neglected temperature effect on H_2O vapor.

$(7.7 \pm 1.4) \times 10^5$ cm^{-3} and a lifetime for CH_3CCl_3 of 6.3 (+1.2, −0.9) years (*50*). The simplicity of the ALE-GAGE concept has been compromised somewhat by the discoveries that the ocean takes up a small amount of CH_3CCl_3 (*51*) and that derived OH depends on the choice of model (*46*). The ALE-GAGE data have been used to infer a trend in global OH concentrations from 1978 to 1990 (+1.0 ± 0.8% year^{-1}), although this conclusion depends strongly on inferred OH for a couple of relatively extreme years (*52*). A positive trend in global OH would be consistent with a tropical O_3 increase or a H_2O vapor increase from temperatures increasing during the past decade. An increase in global OH levels could also account for a diminishing rate of atmospheric CH_4 increase (*33*), that is, a decline in CH_4 lifetime.

What do models say about likely trends in OH? The answer depends on the assumed distribution of CH_4, CO, NO_x, and NMHC emissions. Current increases in CH_4 and CO concentrations would imply that O_3 concentrations are increasing and OH concentrations are decreasing over time if NO_x and NMHC emissions are unperturbed. There is no way to track OH by measurements back several hundred years to preindustrial conditions. The only observational constraint is given by CH_4 concentrations in ice cores. Modelers have found that CH_4 levels do not narrowly define CO, NO_x, and NMHC emissions that also affect OH (*53*). There is consensus that most of the change in CH_4 since 1700 has been driven by increases in CH_4 sources and that lifetime increases (declining OH) are responsible for 10 to 20% of the change (*12, 14, 54*).

The consensus of several model evaluations of preindustrial OH concentrations (Table 1) is that OH concentrations have decreased globally since the start of preindustrial times with a continuing present-day loss of OH likely over remote Southern Hemisphere regions where NO_x levels are low (*6*). Both 2D and 3D model calculations show that, globally, the present OH concentrations are 10 to 30% lower than the values in the period 1200 to 1800.

Several models have attempted to simulate conditions of the Last Glacial Maximum (LGM, 18,000 years ago) using the ice-core record of CH_4 concentrations and temperatures and assumed emissions of CO, NO, and NMHC that are based on scaling back contemporary budgets (*25, 55, 56*). At 18,000 years ago atmospheric CH_4 concentrations were 350 ± 30 ppbv compared to 1700 to 1800 ppbv today (*57*). The lower temperatures are assumed to produce an environment lower in water vapor than present day, hence a slower rate of OH formation (by R2). The model results suggest that OH concentrations were higher than present-day results, but not much greater than OH concentrations from 1200 to 1800 (Table 1). The tendency for lower CH_4 and CO concentrations to coexist with higher OH concentrations in the LGM is offset by a cooler atmosphere, which cuts down the rate of OH formation from O_3 photodissociation. Although these results are instructive about CH_4-CO-OH feedbacks (*25, 55, 58*), the reliability of model estimates of OH in ancient atmospheres is severely restricted by lack of chemical data and uncertain assessments of biogenic NO, CO, and NMHC fluxes during a cooler climate. Ideally, it would be desirable to infer historical OH by using a model and ice-core measurements of a trace gas uncoupled from the CH_4-CO-NO_x-OH-NMHC-O_3 cycle.

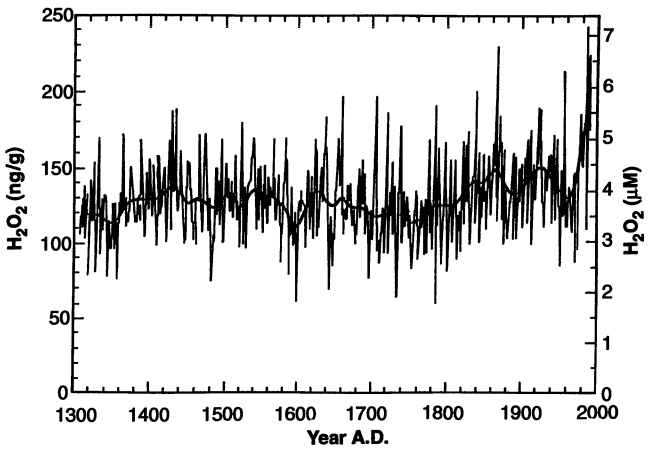

Fig. 7. Increase in H_2O_2 dissolved in the Eurocore sample from Summit, Greenland (72°N) (*61*). A similar increase appears in two recent drillings at Dye 3 in south Greenland. The observation that ice-core H_2O_2 levels in Antarctica are much lower than at Greenland may result from differences in temperature, precipitation, and ice accumulation rates rather than from atmospheric H_2O_2 concentrations (*61*). [Reprinted by permission from (*61*). Copyright © 1991 Macmillan Magazines Ltd.]

Hydrogen peroxide. Hydrogen peroxide, which forms in gaseous and condensed phases and is subject to washout by precipitation, is not easily monitored (*59*). A record of changes in background H_2O_2 concentrations has been derived from analysis of H_2O_2 in ice cores at remote permafrost locations in Greenland and Antarctica (*60*). Interpretation of the ice-core record is complicated by handling of the sample, long-term instability of H_2O_2 in ice, and the relation of atmospheric H_2O_2 concentrations to the ice accumulation process (*60, 61*). Two recently drilled cores in Greenland, one at 65°N and one at 72°N, show distinct temporal trends (Fig. 7). In the Eurocore sample that goes back to 1300, ice formed in the first 400 years shows a stable mean H_2O_2 concentration; from 1700 to 1989 there was a 50% increase in dissolved H_2O_2, with most of the increase during the past 20 years. In contrast, sampling of ice at Siple Station, Antarctica, shows no trend over the past 83 years, but this may reflect a problem with H_2O_2 stability in the samples (*61*). If the recent decreases in surface O_3 at the summertime South Pole (*38*) are due to more ultraviolet light, the loss of O_3 would be expected to give more OH, HO_2, and H_2O_2 (*16*).

Probable Future Oxidant Changes

Future changes in atmospheric oxidizing capacity are predicted by models that calculate O_3, OH, and H_2O_2 distributions based on assumed scenarios of trace gas emissions (*62*). Although many chemical processes and feedback mechanisms are understood, the task of making reliable oxidant predictions on a global scale continues to be complicated by several factors. There are large uncertainties in budgets for NO_x,

Table 2. Model predictions of global O_3 increases with continued high-growth scenarios. GISS, Goddard Institute for Space Studies; AMAC, Assessment Model for Atmospheric Composition; GSFC, Goddard Space Flight Center; NH, Northern Hemisphere; SH, Southern Hemisphere.

Model and type	Reference	Annual increase in tropical O_3 (%)
GISS/AMAC* (0D+rad.)	(*76*)	+0.5
GSFC* (multi-1D)	(*15*)	+0.5
University of Oslo* (2D)	(*75*)	+0.2
Harwell (2D)	(*28*)	Tropics: +0.6; NH: 1.5
Cambridge University (2D)	(*30*)	SH: +0.6; NH: 1.5
Max Planck (1D+rad.)	(*66*)	SH: +0.2; NH: 1

*Models ran the same scenarios in an intercomparison study (*62*).

CO, and hydrocarbon emissions that lead to oxidant formation. For example, the sharp increase in CH_4 observed over the past 30 years has slowed down for the past few years. This may be temporary or it could mean that CH_4 source increases are slowing down. On a global basis the other O_3 precursors—NMHC, CO, and NO—have sources that are roughly half natural and half anthropogenic. Thus, it is difficult to predict future growth in emissions from energy consumption, deforestation, biomass burning, and aircraft.

Models for the assessment of future tropospheric composition need to be computationally efficient and validated with observations, which are uneven in coverage, even for O_3. Three-dimensional chemical-transport models are not yet practical for running multiple scenarios. Although several 2D tropospheric models have been developed for oxidant assessments (*26–30*), there is not an intercompared set of models for estimating uncertainty limits on projections (*63*). Furthermore, doubts remain about whether 2D models can be validated, given extreme regional variability in sources. Finally, tropospheric oxidants will respond to processes associated with stratospheric O_3 depletion and climate change. Potential effects on oxidants from a warmer climate are presumably both positive and negative in direction, but the net forcings are unknown (*15, 16, 64–66*).

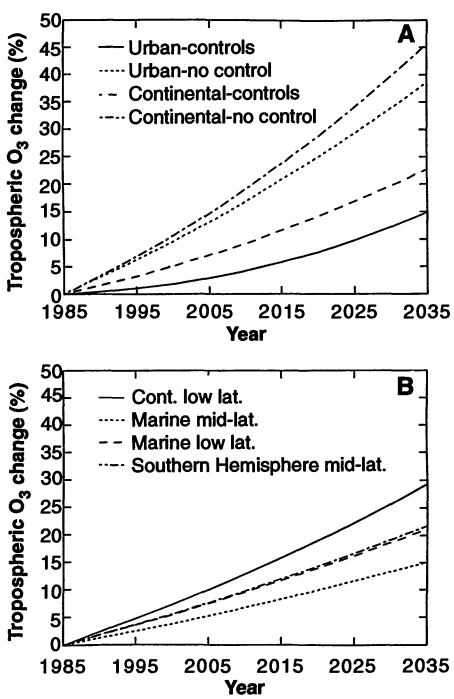

Fig. 8. Percentage change in tropospheric O_3 (column-integrated from 0 to 15 km) calculated with a 1D model that simulates chemically distinct regions [four each in (**A**) and (**B**)]. A moderately high growth rate scenario [ICF scenario 8 in (*15*) and (*62*)] is illustrated. Mean growth rates for emissions are CH_4, +1.3% year^{-1}; NO, +0.5% year^{-1}; CO, +0.06% year^{-1}; predicted increases in CO and NO concentrations are not uniformly distributed over all regions. [Adapted from (*15*)]

Ozone. There is little doubt that continuing growth in emissions of CH_4, NO, CO, and hydrocarbons will tend to increase tropospheric O_3. The questions are how rapidly and where will maximum and minimum growth areas be? Projections of emissions are usually prepared for policy-makers and are based on econometric models that use data for population growth, energy and food demand, land-use programs, and effects of shifting technological options. Emissions growth rates similar to today's define "business-as-usual" scenarios; this means increases of 1 to 2% year^{-1} in total (global) emissions of anthropogenic CH_4, CO, NO, and NMHC.

A number of model studies have been conducted to predict tropospheric oxidant changes over the next 30 to 100 years (Table 2). The range in projected O_3 increases reflects different rates of increase for CH_4, CO, and NO emissions and different geographical distributions of sources for these gases, including in some cases, lightning and upper tropospheric aircraft sources of NO_x (*46, 67, 68*). A typical business-as-usual type scenario with a global mean NO_x increase of 0.5 to 0.6% year^{-1} shows that tropospheric O_3 will increase 0.5% year^{-1}. However, in regions where NO and CO increases are expected to be rapid (over populated parts of Asia, for example), O_3 increases will approach 1% year^{-1} (Fig. 8).

Several model studies have been conducted to estimate the effects of stratospheric O_3 depletion on tropospheric O_3. The effect of increased penetration of ultraviolet radiation into the troposphere (that is, higher photodissociation rates) is to increase O_3 formation in urban regions (*39, 69, 70*). However, on a global basis, lower tropospheric O_3 concentrations are expected to result from stratospheric O_3 depletion because of the dominance of the losses (R1 and R2) in large nonpolluted (low NO_x) regions (*40*). This forcing could oppose the tendency for tropospheric O_3 to increase as CH_4, CO, and NO_x emissions grow. A further moderating effect on a tropospheric O_3 increase could be a warmer climate if the major perturbation is a greater concentration of H_2O vapor. Normally O_3 and H_2O vapor are anticorrelated in the troposphere because higher concentrations of H_2O cause O_3 loss through reactions R1 and R2 (*64, 71*). Thus, in one study a model prediction of tropospheric O_3 increasing 10% over the next 50 years shifts to a 6% increase if stratospheric O_3 declines 10% during the same period (*15*). A temperature increase of 2°C at the surface adds enough H_2O vapor to reduce the projected increase in tropospheric O_3 to only 2% over 50 years. This result is based on a simplified model that does not include possible feedback effects of a warmer climate on biogenic emissions of gases such as CH_4. Localized meteorological changes, for example, additional cloud cover, precipitation, turbulence, and surface characteristics, are also neglected (*72*).

Studies have examined the effects of controlling emissions of O_3 precursor gases (*62*). Controlling emissions of CH_4 and CO can cut the growth rate in tropospheric O_3 approximately in half (Fig. 9). Controlling CH_4 emissions may appeal to policy-makers because CH_4, a greenhouse gas, is expected to contribute ~25% to radiative forcing of climate over the next century (*33*). One study suggests that, if CH_4 emissions were to be stabilized at 1990 levels, the projected global O_3 increase from 1985 to 2100 would be reduced by two-thirds compared to a business-as-usual CH_4 growth rate (*73*).

OH changes. In predicting future atmospheric oxidizing capacity, it is the abundance of OH that is most problematic. The growth of O_3 alone would imply that OH concentrations will also increase, but increasing emissions of CH_4, CO, and NMHC could suppress OH concentrations over large regions (Fig. 10). Background

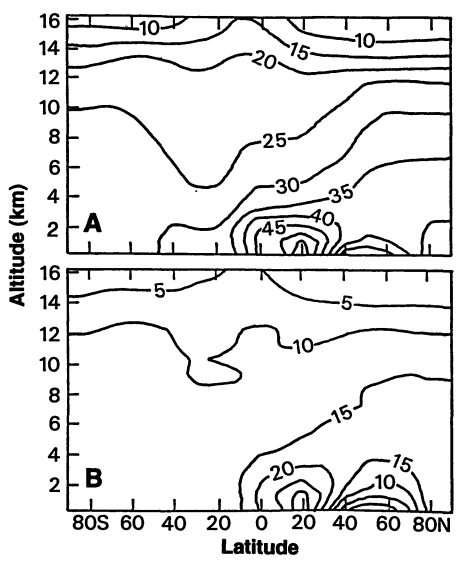

Fig. 9. Percentage change in tropospheric O_3 from 1985 to 2100 calculated with the 2D University of Oslo model. [Adapted from (*75*). Copyright by A. Deepak Publishing] (**A**) High growth scenario is the same as in Fig. 8 but the period of simulation is longer; (**B**) scenario 2 (low growth) in (*15, 62, 75*). Mean growth rates are CH_4, +0.8% year^{-1}; NO, +0.5% year^{-1}; CO, −0.8% year^{-1}. Here the CH_4 growth rate is approximately half the rate as that simulated in (A). The difference in the O_3 increase between (A) and (B) is roughly a factor of 2, illustrating the importance of CH_4 in O_3 formation (*46, 73*).

NO_x and NMHC concentrations are pivotal in determining whether OH concentrations increase or decrease in a region. Longer lived nitrogen-containing compounds (for example, peroxyacetyl nitrate and alkyl nitrates) can supply NO_x to remote locations (*26, 74*).

One 2D model (*75*) shows globally averaged OH concentrations increasing <0.1% $year^{-1}$ from 1985 to 2100 as NO and CH_4 emissions increase (Fig. 10), although OH concentrations in the upper troposphere increase by a factor of 2 or more. However, a zero-dimensional coupled stratosphere-troposphere climate model (*76*) and a multibox 1D model (*15*) both give decreases of 0.3% $year^{-1}$ for the same scenario. When a set of eight scenarios is simulated with these three models, annually averaged rates of change for global OH concentrations are +0.4% $year^{-1}$ for the zero-dimensional model and −0.3% $year^{-1}$ for the other two models (*62*). That the range of OH predictions from these models is greater than the corresponding projections for tropospheric O_3 (Table 2) illustrates the difficulties of predicting future concentrations of OH. Some of the differences among the models result from differences in the treatment of NO emissions.

Future OH concentrations might also be affected by (i) stratospheric O_3 depletion; (ii) a warming climate; or (iii) perturbations to the upper troposphere and lower stratosphere from civilian aircraft. Effects of stratospheric O_3 depletion have been simulated in several models (*40, 64, 77*). In general, the addition of ultraviolet radiation means that tropospheric O_3 will photodissociate and form OH more rapidly. Indeed, one model that simulates increasing CH_4, CO, and NO emissions shows that a 13% global OH loss from 1985 to 2035 would be nearly canceled by a 10% stratospheric O_3 depletion (*15*).

It is more difficult to predict effects of global warming on OH concentrations. In general, a warmer climate at unchanged relative humidity should lead to higher H_2O vapor and OH concentrations, but other perturbations are hard to predict. If mean cloudiness also increases, there could be less ultraviolet radiation reaching the lower troposphere, resulting in lower concentrations of OH. In contrast, greater reflection of ultraviolet radiation in clouds would increase O_3 photodissociation and OH formation above clouds in the mid- and upper troposphere (*78*). Thus, the effect of a modified cloud amount on tropospheric OH concentrations is uncertain.

Calculations of possible effects of civilian aircraft on upper tropospheric oxidants show that, even though NO_x emissions enhance O_3 production, there might be little effect on OH because some OH reacts with NO_x to form HNO_3 (*46, 67, 68*).

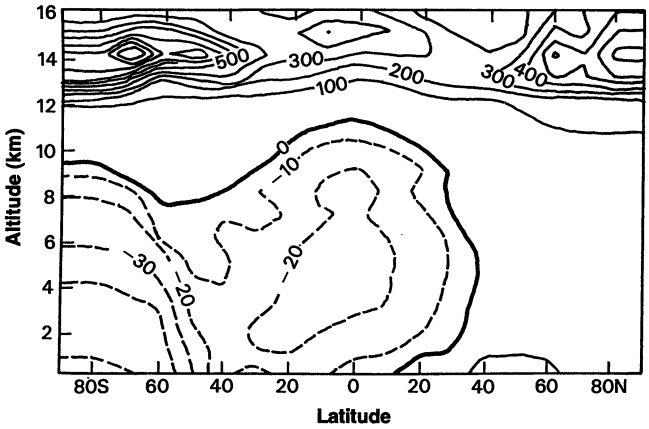

Fig. 10. Percent change in OH from 1985 to 2100 calculated with a 2D model. [From (*75*). Copyright by A. Deepak Publishing] Global mean OH is nearly constant as a result of the near cancellation of positive forcings from increasing NO and controls on CO emissions. Methane is assumed to continue increasing 1% $year^{-1}$.

Hydrogen peroxide. Predictions of future concentrations of H_2O_2 are also sensitive to assumed NO_x distributions. Increases in CH_4, CO, and NMHC emissions convert OH to HO_2 and H_2O_2, except when NO_x concentrations increase rapidly enough for HNO_3 formation to compete with H_2O_2 formation. Thus, a 2D model that assumes global increases in NO emissions predicts that H_2O_2 will decrease at all latitudes (*30*), whereas more moderate scenarios in a multiregion 1D model point to substantial H_2O_2 increases in some regions (*16*). Typical values for business-as-usual scenarios are 50% growth over the next 50 years in all regions except those with highest NO_x concentrations. This is consistent with the recent ice-core record that shows H_2O_2 increasing more than 40% over the past 20 years (*61*). Control of CH_4 and CO emissions would moderate increases in H_2O_2 concentrations. Depletion of stratospheric O_3 and a warmer, moister climate favor H_2O_2 formation at the expense of tropospheric OH and O_3, but not if cloud and precipitation enrichments were to remove the additional H_2O_2 (*16*).

Summary

A review of observations, limited over time and domain, suggests that the earth's oxidizing capacity—defined as the global abundance of tropospheric O_3, OH, and H_2O_2—has changed significantly during the 200 to 300 years of the industrial era. There is good evidence for increasing surface O_3 throughout much of the Northern Hemisphere, ~0.1 to 0.3% $year^{-1}$ over the past century in some locations. More recently, dry-season O_3 concentrations may be increasing in the tropics because of widespread biomass burning.

We can rationalize increases in O_3 concentrations by noting that the abundance of the O_3 precursor CH_4 has increased globally since preindustrial times. Photochemical models show that increasing CH_4 (and CO) concentrations could account for a doubling of background tropospheric O_3 since 1800. The role played by perturbed NO_x and NMHC emissions is harder to quantify because of nonlinearity in O_3 formation.

Trends in the critical oxidant OH are less certain. Increases in CH_4 and CO concentrations over vast regions suggest that the global OH abundance was greater in the preindustrial era than now. Presently, OH continues to be suppressed by increases in CO and CH_4 emissions over much of the Southern Hemisphere, but where urbanization and biomass burning are on the rise increasing O_3 concentrations could lead to higher OH concentrations. A decline in the rate of atmospheric CH_4 increase over the past 3 to 5 years could signal an increase in global OH abundance. It appears that small changes in OH, either positive or negative, should occur in the next century or so. Increases would be beneficial in controlling stratospheric O_3-depleting hydrochlorofluorocarbons, but they would aggravate other environmental problems, for example, rates of acid formation in the troposphere.

Concentrations of H_2O_2 could be increasing at even greater rates than tropospheric O_3, although increases in NO_x emissions tend to counteract increases in atmospheric H_2O_2. Recent increases in H_2O_2 concentrations in Greenland ice cores suggest that increases in CH_4 and CO concentrations will add to the atmospheric burden of this oxidant. The increase in H_2O_2 concentrations could be a sign of OH depletion, representing net conversion of OH to HO_2.

REFERENCES AND NOTES

1. The U.S. Environmental Protection Agency defines a region to be in violation of the air quality standard whenever 2 days in a calendar year register maximum 1-hour averaged O_3 mixing ratios in excess of 120 ppbv.
2. W-C. Wang, J. P. Pinto, Y. Yung, *J. Atmos. Sci.* **37**, 333 (1980); A. A. Lacis, D. J. Wuebbles, J. A. Logan, *J. Geophys. Res.* **95**, 9971 (1990).
3. T. E. Graedel, *Chemical Compounds in the Atmo-*

sphere (Academic Press, New York, 1978).
4. S. A. Penkett, B. M. R. Jones, K. A. Brice, A. E. J. Eggleton, *Atmos. Environ.* **13**, 123 (1979).
5. In urban environments the free radicals NO_3 and HO_2 may be significant oxidants, especially at night. See B. J. Finlayson-Pitts and J. N. Pitts, Jr., *Atmospheric Chemistry: Fundamentals and Experimental Techniques* (Wiley, New York, 1986).
6. I. S. A. Isaksen, in *The Changing Atmosphere: Report of the Dahlem Workshop on the Changing Atmosphere*, F. S. Rowland and I. S. A. Isaksen, Eds. (Wiley-Interscience, New York, 1988), pp. 141–158.
7. M. Prather and C. Spivakovsky, *J. Geophys. Res.* **95**, 18723 (1990).
8. T. E. Graedel and C. J. Weschler, *Rev. Geophys. Space Phys.* **19**, 505 (1981); W. L. Chameides and D. D. Davis, *J. Geophys. Res.* **87**, 4863 (1982).
9. H. Levy III, *Planet. Space Sci.* **20**, 919 (1972); P. J. Crutzen, *Pure Appl. Geophys.* **106–108**, 1385 (1973). The sequence of reactions R1 through R9, and analogous processes starting with OH attack on NMHC are known collectively as "smog" reactions. See M. W. Gery *et al.*, *J. Geophys. Res.* **94**, 12935 (1989); F. W. Lurmann *et al.*, *ibid.* **91**, 10905 (1986); W. R. Stockwell *et al.*, *ibid.* **95**, 16343 (1990).
10. D. H. Ehhalt, in *The Changing Atmosphere: Report of the Dahlem Workshop on the Changing Atmosphere*, F. S. Rowland and I. S. A. Isaksen, Eds. (Wiley-Interscience, New York, 1988), pp. 25–32; R. A. Rasmussen and M. A. K. Khalil, *J. Geophys. Res.* **86**, 9826 (1981); D. R. Blake and F. S. Rowland, *J. Atmos. Chem.* **4**, 43 (1986).
11. H. Craig and C. C. Chou, *Geophys. Res. Lett.* **9**, 1221 (1982); R. A. Rasmussen and M. A. K. Khalil, *J. Geophys. Res.* **89**, 11599 (1984); B. Stauffer, G. Fischer, A. Neftel, H. Oeschger, *Science* **229**, 1386 (1985).
12. W. L. Chameides, S. C. Liu, R. J. Cicerone, *J. Geophys. Res.* **82**, 1795 (1977); N. D. Sze, *Science* **195**, 673 (1977); J. S. Levine, C. P. Rinsland, G. M. Tennille, *Nature* **318**, 254 (1985).
13. S. Hameed, J. P. Pinto, R. W. Stewart, *J. Geophys. Res.* **84**, 763 (1979).
14. A. M. Thompson and R. J. Cicerone, *ibid.* **91**, 10853 (1986).
15. A. M. Thompson, M. A. Huntley, R. W. Stewart, *ibid.* **95**, 9829 (1990).
16. ———, *Atmos. Environ. Part A* **25**, 1837 (1991).
17. Hydroxyl reacts efficiently with oxygenated hydrocarbons, including radicals, peroxides, aldehydes, and acyl compounds; a compilation of rate coefficients for OH attack on organic compounds is R. Atkinson, Ed., *Journal of Physical and Chemical Reference Data, Monograph 1* (American Institute of Physics, New York, 1989).
18. S. C. Liu *et al.*, *J. Geophys. Res.* **92**, 4191 (1987).
19. X. Lin, M. Trainer, S. C. Liu, *ibid.* **93**, 15879 (1988).
20. J. A. Leone and J. H. Seinfeld, *Atmos. Environ.* **19**, 437 (1985); W. R. Stockwell, *ibid.* **20**, 1615 (1986); A. M. Hough, *J. Geophys. Res.* **93**, 3789 (1988); M. C. Dodge, *ibid.* **94**, 5121 (1989).
21. Regional-scale models developed for acid deposition address some of these requirements, for example, J. S. Chang *et al.*, *J. Geophys. Res.* **92**, 14681 (1987).
22. J. Lilieveld and P. J. Crutzen, *Nature* **343**, 227 (1990).
23. W. B. DeMore *et al.*, Eds., "Chemical kinetics and photochemical data for use in stratospheric modeling: NASA Kinetics Panel Evaluation No. 9" (NASA/JPL Publ. 90-1, Jet Propulsion Laboratory, Pasadena, CA, 1990).
24. A. M. Thompson and R. W. Stewart, *J. Geophys. Res.* **96**, 13089 (1991). The uncertainty in a model calculation of ambient OH from a set of high-precision measurements of O_3, CO, and NO_x may be reduced to 15 to 20%.
25. Y. Lu and M. A. K. Khalil, *Chemosphere* **23**, 397 (1991).
26. P. J. Crutzen and L. T. Gidel, *J. Geophys. Res.* **88**, 6641 (1983); M. Kanakidou, H. B. Singh, K. M. Valentin, P. J. Crutzen, *ibid.* **96**, 15395 (1991).
27. I. S. A. Isaksen and O. Hov, *Tellus Ser. B* **39**, 271 (1987).
28. A. M. Hough and R. G. Derwent, *Nature* **344**, 645 (1990).
29. D. J. Wuebbles, P. S. Connell, K. E. Grant, R. Tarp, K. E. Taylor, *Report UCRL-21178* (Lawrence Livermore National Laboratory, Livermore, CA, 1987).
30. K. S. Law and J. A. Pyle, *Atmos. Environ. Part A* **25**, 1863 (1991).
31. A 2D meridionally averaged model is described in S. Solberg, I. S. A. Isaksen, R. B. Chatfield, in *Ozone in the Atmosphere*, R. D. Bojkov and P. Fabian, Eds. (A. Deepak, Hampton, VA, 1989), pp. 548–551.
32. M. Kanakidou and P. J. Crutzen, *Chemosphere*, in press; P. H. Zimmermann, J. Feichter, H. K. Rath, P. J. Crutzen, W. Weiss, in *Air Pollution Modeling and Its Application*, H. Van Dop, Ed. (Plenum, New York, 1988), vol. 6, pp. 593–607.
33. For discussion of the roles of O_3 and OH in climate change, see R. T. Watson, H. Rodhe, H. Oeschger, U. Siegenthaler, in *Climate Change: The IPCC (Intergovernmental Panel on Climate Change) Assessment*, J. T. Houghton, G. J. Jenkins, J. J. Ephraums, Eds. (Cambridge Univ. Press, Cambridge, 1990), chap. 1.
34. R. B. Chatfield and P. J. Crutzen, *J. Geophys. Res.* **89**, 7111 (1984); R. R. Dickerson *et al.*, *Science* **235**, 460 (1987); K. E. Pickering *et al.*, *J. Geophys. Res.* **95**, 14049 (1990).
35. R. D. Bojkov, *J. Climate Appl. Meteorol.* **25**, 343 (1986). A new report of surface O_3 doubling in South America from the 1880s to the present is in S. Sandroni, D. Anfossi, S. Viarengo, *J. Geophys. Res.* **97**, 2535 (1992).
36. A. Volz and D. Kley, *Nature* **332**, 240 (1988).
37. *Summary Rep. 1989: No. 18* (NOAA/CMDL, Boulder, CO, 1990), pp. 40–49.
38. R. C. Schnell *et al.*, *Nature* **351**, 726 (1991).
39. S. Madronich, *Geophys. Res. Lett.* **19**, 37 (1992); P. J. Crutzen, *Nature* **356**, 104 (1992).
40. S. C. Liu and M. Trainer, *J. Atmos. Chem.* **6**, 221 (1988).
41. A. M. Thompson, *Nature* **352**, 282 (1991).
42. J. Fishman, C. E. Watson, J. C. Larsen, J. A. Logan, *J. Geophys. Res.* **95**, 3599 (1990). Typical values for total O_3 range from 250 DU over the tropical Pacific to 450 DU or more at high latitudes except during the period of the Antarctic O_3 hole, when TOMS has sometimes measured <120 DU. Eighty percent or more of the total O_3 column is in the stratosphere.
43. J. Fishman, K. Fakhruzzaman, B. Cros, D. Nganga, *Science* **252**, 1693 (1991). This paper includes data through 1989. Figure 6 includes data from 1990 and uses Version 6.0 of the TOMS archive instead of Version 5.0. The newer version of the TOMS Archive results in an increase of the tropospheric residual amounts of ~11%. The maximum off the western African coast may include some artifact O_3 because of increased reflectivity over marine stratocumulus clouds.
44. J. Fishman, personal communication. The possible importance of biomass burning was pointed out by P. J. Crutzen, L. E. Heidt, J. P. Krasnec, W. H. Pollock, and W. Seiler [*Nature* **282**, 253 (1979)].
45. R. S. Stolarski, P. Bloomfield, R. D. McPeters, J. Herman, *Geophys. Res. Lett.* **18**, 1015 (1991).
46. The most recent stratospheric O_3 Assessment Report discusses the roles of tropospheric OH and O_3 in stratospheric chemistry: I. S. A. Isaksen *et al.*, in *Scientific Assessment of Ozone Depletion: 1991* (*Rep. 25*, World Meteorological Organization–United Nations Environment Programme, Geneva, Switzerland, 1992), chap. 5.
47. H.-P. Dorn, J. Callies, U. Platt, D. H. Ehhalt, *Tellus Ser. B* **40**, 437 (1988); A. Hofzumahaus *et al.*, *Atmos. Environ. Part A* **25**, 2017 (1991); G. H. Mount, *J. Geophys. Res.* **97**, 2427 (1992).
48. I. S. Leifer, D. J. Tanner, F. L. Eisele, *Eos* **72**, 99 (1991). An intercomparison of two OH measurement techniques appears in this issue; see G. H. Mount *et al.*, *Science* **256**, 1187 (1992) and W. Brune, *ibid.*, p. 1154.
49. R. Prinn *et al.*, *Science* **238**, 945 (1987).
50. D. M. Cunnold and R. G. Prina, *J. Geophys. Res.* **96**, 17392 (1992); difficulties in calibration and constraint of lifetime are discussed by C. M. Spivakovsky, *ibid.*, p. 17395.
51. J. J. Butler *et al.*, *ibid.*, p. 22347.
52. R. Prinn *et al.*, *ibid.* **97**, 2445 (1992).
53. A. M. Thompson, J. A. Chappellaz, I. Y. Fung, T. L. Kucsera, in preparation.
54. M. A. K. Khalil and R. A. Rasmussen, *Atmos. Environ.* **19**, 397 (1985).
55. J. P. Pinto and M. A. K. Khalil, *Tellus Ser. B* **43**, 347 (1991).
56. M. B. McElroy, in *The Environmental Record in Glaciers and Ice Sheets*, H. Oeschger and C. C. Langway, Jr., Eds. (Wiley, London, 1989), pp. 363–377.
57. B. Stauffer, E. Lochbronner, H. Oeschger, J. Schwander, *Nature* **332**, 812 (1988); D. Raynaud, J. Chappellaz, J. M. Barnola, Y. S. Korotkevich, *ibid.* **333**, 665 (1988).
58. P. D. Guthrie, *Global Biogeochem. Cycles* **4**, 287 (1989); Y. Lu and M. A. K. Khalil, in preparation.
59. D. W. Gunz and M. R. Hoffmann, *Atmos. Environ. Part A* **24**, 1601 (1990).
60. A. Neftel, P. Jacob, D. Klockow, *Nature* **311**, 43 (1984); A. Sigg and A. Neftel, *Ann. Glaciol.* **10**, 157 (1988); A. Sigg, T. Staffelbach, A. Neftel, *J. Atmos. Chem.* **14**, 223 (1992).
61. A. Sigg and A. Neftel, *Nature* **351**, 557 (1991).
62. D. A. Lashof and D. A. Tirpak, Eds., *Policy Options for Stabilizing Global Climate: Report to Congress* (USEPA Publ. 21P-2003.1 and 21P-2003.3, Environmental Protection Agency, Washington, DC, 1990). In this report the models described in (*15, 75,* and *76*) were intercompared; each model was used to run a set of eight scenarios for CH_4, CO, and NO emissions from 1985 to 2050.
63. Roughly a dozen 2D models for stratospheric assessment purposes have been intercompared by running the same scenarios. C. H. Jackman, R. K. Seals, Jr., M. J. Prather, Eds., "Two-dimensional comparison of stratospheric models," *NASA Conference Publication 3042* (NASA, Washington, DC, 1989). Despite the simplifications of heterogeneous chemistry and 2D transport, the scientific community accepts the use of these models for U.S. and international assessment and policy studies because they are able to reproduce observations of total O_3 reasonably well. See (*45, 46*).
64. A. M. Thompson, R. W. Stewart, M. A. Owens, J. A. Herwehe, *Atmos. Environ.* **23**, 519 (1989).
65. Few models have looked at a range of interactions among perturbed climate, troposphere, and stratosphere. See D. J. Wuebbles, K. E. Grant, P. S. Connell, and J. E. Penner [*J. Air Pollut. Control Assoc.* **39**, 22 (1989)] and D. J. Wuebbles and J. E. Penner ["Sensitivity of Urban/Regional Chemistry to Climate Change: Report of the Workshop, 17–18 February 1988" (*Rep. UCRL-99436* (Lawrence Livermore National Laboratory, Livermore, CA, 1989).
66. C. Bruhl and P. J. Crutzen, *Climate Dyn.* **2**, 173 (1988).
67. Studies have examined the impact of aircraft emissions on upper tropospheric O_3 (*46, 68*). On the basis of the channel model (*31*), it is estimated that typical NO emissions from civilian aircraft maintain upper tropospheric O_3 levels 12% above levels consistent with no aircraft. J. P. Beck, C. E. Reeves, F. A. A. M. de Leeuw, S. A. Penkett, *Atmos. Environ. Part A* **26**, 17 (1992).
68. R. G. Derwent, *Atmos. Environ.* **16**, 1997 (1982); S. C. Liu *et al.*, *J. Geophys. Res.* **85**, 7546 (1980); C. Johnson, J. Henshaw, G. McInnes, *Nature* **354**, 69 (1992).
69. M. W. Gery, in *Environmental Effects of Ozone Depletion: 1991 Update* (United Nations Environment Programme, November 1991, available from the Environmental Protection Agency, Washington, DC, Publication RD-682D).
70. There are clearly increases in surface ultraviolet light associated with the Antarctic ozone hole [D. Lubin, J. E. Frederick, A. J. Krueger, *J. Geophys. Res.* **94**, 8491 (1989)], but no definite evidence at mid-latitudes. See C. Bruhl and P. J. Crutzen,

Geophys. Res. Lett. **16**, 703 (1989).
71. D. Kley *et al.*, in *Global and Regional Environmental Atmospheric Chemistry: Proceedings of the International Conference on Global and Regional Environmental Atmospheric Chemistry* (Department of Energy Conference 890525, 1989, available from the National Technical Information Service, Springfield, VA), p. 9.
72. D. Rind, R. Suozzo, N. K. Balanchandran, M. J. Prather, *J. Atmos. Sci.* **47**, 475 (1990).
73. K. B. Hogan, J. S. Hoffman, A. M. Thompson, *Nature* **354**, 181 (1991); A. M. Thompson, K. B. Hogan, J. S. Hoffman, *Atmos. Environ.*, in press.
74. C. S. Atherton and J. E. Penner, *J. Geophys. Res.* **95**, 14027 (1990).
75. I. S. A. Isaksen, T. Berntsen, S. Solberg, in *Ozone in the Atmosphere*, R. D. Bojkov and P. Fabian, Eds. (A. Deepak, Hampton, VA, 1989), pp. 576–579.
76. M. J. Prather, Ed., "An assessment model for atmospheric composition" (*NASA Conf. Publ. 3023*, NASA, Washington, DC, 1989).
77. S. Madronich and C. Granier, *Geophys. Res. Lett.* **19**, 465 (1992).
78. A. M. Thompson, *J. Geophys. Res.* **89**, 1341 (1984); S. Madronich, *ibid.* **92**, 9740 (1987).
79. S. A. Penkett and K. A. Brice, *ibid.* **319**, 655 (1986).
80. J. A. Logan, *J. Geophys. Res.* **90**, 10463 (1985). An update for the North American data is in J. A. Logan, in *Tropospheric Ozone*, I. S. A. Isaksen, Ed. (North Atlantic Treaty Organization Advanced Study Institutes, Reidel, Dordrecht, Holland, 1988), pp. 327–344.
81. Locations of sites: Barrow (71°N, 157°W); Mauna Loa (19.5°N, 156°W); Samoa (14°S, 171°W); South Pole (90°S, 0). See (*36*); S. J. Oltmans and W. D. Komhyr, *J. Geophys. Res.* **91**, 5229 (1986).
82. K. M. Valentin, thesis, Johannes-Gutenburg University, Mainz (1990).
83. P. J. Crutzen and P. H. Zimmermann, *Tellus Ser. B* **43**, 136 (1991).
84. The following people have been generous with reports of recent work: C. Bruhl, J. Fishman, I. S. A. Isaksen, M. Kanakidou, M. A. K. Khalil, K. Law, Y. Lu, A. Neftel, J. Pinto, M. Prather, and R. Prinn. M. Kanakidou, J. Logan, and W. Stockwell made helpful comments on the manuscript. Some of the model comparisons (Tables 1 and 2) grew out of the United Nations Environmental Programme–World Meteorological Organization Ozone Assessment Group Workshop (London, June 1991) and a North Atlantic Treaty Organization Advanced Research Workshop on Methane (Mt. Hood, Oregon, October 1991). My research on oxidizing changes is supported by NASA Programs in Earth Observing Systems and Tropospheric Chemistry and by the U.S. Environmental Protection Agency.

Molecular Epidemiology of HIV Transmission in a Dental Practice

Chin-Yih Ou, Carol A. Ciesielski, Gerald Myers, Claudiu I. Bandea, Chi-Cheng Luo, Bette T. M. Korber, James I. Mullins, Gerald Schochetman, Ruth L. Berkelman, A. Nikki Economou, John J. Witte, Lawrence J. Furman, Glen A. Satten, Kersti A. MacInnes, James W. Curran, Harold W. Jaffe, Laboratory Investigation Group,* Epidemiologic Investigation Group†

Human immunodeficiency virus type 1 (HIV-1) transmission from infected patients to health-care workers has been well documented, but transmission from an infected health-care worker to a patient has not been reported. After identification of an acquired immunodeficiency syndrome (AIDS) patient who had no known risk factors for HIV infection but who had undergone an invasive procedure performed by a dentist with AIDS, six other patients of this dentist were found to be HIV-infected. Molecular biologic studies were conducted to complement the epidemiologic investigation. Portions of the HIV proviral envelope gene from each of the seven patients, the dentist, and 35 HIV-infected persons from the local geographic area were amplified by polymerase chain reaction and sequenced. Three separate comparative genetic analyses—genetic distance measurements, phylogenetic tree analysis, and amino acid signature pattern analysis—showed that the viruses from the dentist and five dental patients were closely related. These data, together with the epidemiologic investigation, indicated that these patients became infected with HIV while receiving care from a dentist with AIDS.

Increasingly, molecular biologic techniques have been used to study the epidemiology of infectious diseases. For viral infections of humans, techniques to analyze viral genetic sequence information, such as oligonucleotide fingerprinting of RNA genomes with ribonuclease, mapping of DNA genomes with restriction endonucleases, and genomic sequencing, have been used to study viral transmissions from person to person, within communities, and between countries (*1*). Requisite to such studies is the existence of viral genetic variation; the greater the variation, the greater the power of the methods to distinguish strains of the virus. For a virus with substantial genomic variation, identification of strains with a high degree of genetic relatedness may imply an epidemiologic linkage between persons infected with these strains.

The human immunodeficiency virus (HIV) has a high mutation rate (*2*, *3*), such that HIVs from different individuals are found to be genetically distinct (*3*). In this article, we describe the use of genomic sequencing to investigate a cluster of HIV infections in a Florida dental practice. The high degree of genetic relatedness observed among the HIV strains from a dentist with acquired immunodeficiency syndrome (AIDS) and five of his infected patients supports the epidemiologic investigation that indicated that these patients became infected with HIV while receiving dental care.

Epidemiologic Investigation

In July 1990, we reported that a young woman with AIDS (patient A) had most likely acquired her HIV-1 infection while undergoing invasive dental procedures by a Florida dentist with AIDS (*4*). Following publication of the report, the dentist publicly requested that his former patients be tested for HIV infection. Among approximately 1100 persons whose blood was tested by the Florida Department of Health and Rehabilitative Services (HRS), two patients (patients B and C) were found to be HIV-positive. An additional infected patient (patient D) was ascertained by HRS through cross matching a list of the dentist's former patients with the Florida AIDS case registry. Two other patients of the dentist (patients E and G) contacted the Centers for Disease Control (CDC) to report that they were HIV-infected. A former sex partner named by patient E was found to be HIV-infected and had also been a patient of the dentist (patient F). Characteristics of these seven infected patients and the dentist are included in Table 1.

Patient D had previously been reported

C.-Y. Ou, C. A. Ciesielski, C. I. Bandea, C.-C. Luo, G. Schochetman, R. L. Berkelman, G. A. Satten, J. W. Curran, and H. W. Jaffe are in Division of HIV/AIDS, National Center for Infectious Diseases, Centers for Disease Control, Atlanta, GA 30333. G. Myers, B. T. M. Korber, and K. A. MacInnes are in the Theoretical Division, Los Alamos National Laboratory, Los Alamos, NM 87545. J. I. Mullins is in the Department of Microbiology and Immunology, Stanford University School of Medicine, Stanford, CA 94305. A. N. Economou and J. J. Witte are in the Florida Department of Health and Rehabilitative Services, Tallahassee, FL 32399. L. J. Furman is in the Division of Oral Health, National Center for Prevention Services, Centers for Disease Control, Atlanta, GA 30333.

*J. Moore, Y. Villamarzo, and C. Schable, Division of HIV/AIDS and E. G. Shpaer, Department of Microbiology and Immunology, Stanford University School of Medicine.

†T. Liberti and S. Lieb, Florida Department of Health and Rehabilitative Services (HRS); R. Scott, J. Howell, R. Dumbaugh, A. Lasch, Florida HRS District 9; B. Kroesen and L. Ryan, Martin County Public Health Unit, Florida HRS; K. Bell, V. Munn, D. Marianos, and B. Gooch, Centers for Disease Control.